CrossMark

J. Fluid Mech. (2018), *vol.* 846, *pp.* 999–1022. © Cambridge University Press 2018
doi:10.1017/jfm.2018.322

On the weakly nonlinear seakeeping solution near the critical frequency

Chengxi Li[1] **and Yuming Liu**[1,†]

[1]Department of Mechanical Engineering, Massachusetts Institute of Technology, Cambridge, MA 02139, USA

(Received 28 September 2017; revised 11 April 2018; accepted 11 April 2018; first published online 11 May 2018)

We study theoretically and numerically the nonlinear seakeeping problem of a submerged or floating body translating with constant forward speed U parallel to the undisturbed free surface while at the same time undergoing a small oscillatory motion and/or encountering small-amplitude waves at frequency ω. It is known that at the critical frequency corresponding to $\tau \equiv \omega U/g = 1/4$, where g is the gravitational acceleration, the classical linear solution is unbounded for a single point source, and the inclusion of third-order free-surface nonlinearity due to cubic self-interactions of waves is necessary to remove the associated singularity. Although it has been shown that the linear solution is in fact bounded for a body with full geometry rather than a point source, the solution still varies sharply near the critical frequency. In this work, we show theoretically that for a submerged body, the nonlinear correction to the linear solution due to cubic self-interactions of resonant waves in the neighbourhood of $\tau = 1/4$ is of first order in the wave steepness (or body motion amplitude), which is the same order as the linear solution. With the inclusion of nonlinear effects in the dispersion relation, the wavenumbers of resonant waves become complex-valued and the resonant waves become evanescent, with their amplitudes vanishing with the distance away from the body. To assist in understanding the theory, we derive the analytic nonlinear solution for the case of a submerged two-dimensional circular cylinder in the neighbourhood of $\tau = 1/4$. Independent numerical simulations confirm the analytic solution for the submerged circular cylinder. Finally, we also demonstrate by numerical simulations that similar significant nonlinear effects for a surface-piercing body exist in the neighbourhood of $\tau = 1/4$.

Key words: surface gravity waves, waves/free-surface flows, wave–structure interactions

1. Introduction

We consider the seakeeping problem of a translating body with oscillatory motions (or under incident waves) in the presence of a free surface. Due to its importance in the design and safe operation of ships and marine structures, this problem has been the subject of a large number of investigations. Since the oscillatory motions are often small compared with the body dimensions, the majority of studies focus on

† Email address for correspondence: yuming@mit.edu

https://doi.org/10.1017/jfm.2018.322 Published online by Cambridge University Press

the linearized problem (e.g. Newman 1978; Nakos & Sclavounos 1990). Satisfactory predictions can generally be obtained except in the neighbourhood of wave resonance given by the frequency (ω) and forward speed (U) combination $\tau \equiv U\omega/g = 1/4$, where g is the gravitational acceleration. Inclusion of nonlinear free-surface effects may suppress or shift the wave resonance through changes to the dispersion relation, leading to distinctively different characteristics of the solution. The present work aims to understand through theoretical analysis and direct numerical simulations the characteristic features of the nonlinear seakeeping solution in the neighbourhood of the critical frequency $\tau = 1/4$ for real bodies.

For a point source, the classical linear solution derived by Haskind (1954) becomes unbounded at $\tau = 1/4$. The solution for a body with non-zero volume can be represented by an appropriate distribution of such sources (e.g. Havelock 1958; Wehausen & Laitone 1960; Maruo 1967; Sclavounos, Nakos & Huang 1993). It is commonly believed that the resulting problem for the body must likewise be singular at $\tau = 1/4$, which suggests that difficulties may be inherent in the linear problem. Physically, in two-dimensional (2D) cases, when $\tau < 1/4$, four waves are generated and three distinct waves propagate downstream from the body while one propagates upstream, whereas for $\tau > 1/4$, only two downstream waves are left. The group velocities of the two waves that disappear at $\tau > 1/4$ would approach U as $\tau \to 1/4$. As a result, the associated energy can no longer be radiated away, and the amplitudes of these wave components tend to grow indefinitely. These two waves become resonant at $\tau = 1/4$. Similar wave resonance also exists in shallow water (Tyvand & Torheim 2012) or a two-layer fluid (Alam, Liu & Yue 2009) and in the presence of a shear current (Li & Ellingsen 2016).

Through asymptotic analysis, Liu & Yue (1993) showed that the linear solution of the seakeeping problem for a body is finite at $\tau = 1/4$ if a certain geometric condition is satisfied. For a submerged body, a necessary and sufficient condition is that the body must have non-zero volume, while the sufficient condition for a surface-piercing body has a geometric interpretation similar to that of John (1950). The theoretical prediction is consistent with the numerical solution by the boundary integral equation method in the frequency domain for the cases of submerged circular and elliptical cylinders (Grue & Palm 1985; Mo & Palm 1987). Kring (1998) obtained a finite linear seakeeping solution through the critical frequency for realistic ship hulls by means of numerical simulation in the time domain with a Rankine source boundary-element method. Later, Palm & Grue (1999) found that when the wake effect is accounted for, the solution for a thin 2D foil is also finite at the critical frequency. Zhu, Liu & Yue (2006) also found the finite solution for a three-dimensional (3D) hydrofoil. Unlike a single point source, the source distributed on the body is constrained to satisfy the finite body boundary condition. This results in the finite solution at $\tau = 1/4$ for a non-zero volume body or a thin hydrofoil despite the influence of wave resonance. Due to weak radiation of the resonant waves near the critical frequency, however, the (finite) linear solution is still found to be quite large and varies sharply near $\tau = 1/4$ (Grue & Palm 1985; Mo & Palm 1987; Liu & Yue 1993; Palm & Grue 1999). Therefore, nonlinear effects are generally expected to play an important role in the seakeeping solution near the critical frequency.

Nonlinear wave–wave interactions are known to play a prominent role in the dynamics of wave resonance. They can cause energy transfer among interacting wave components (e.g. Alam, Liu & Yue 2011) and modifications of wave phase/group velocities, which may enhance or suppress the resonance (e.g. Dagan & Miloh 1980, 1982; Akylas 1984). For a single point source, Dagan & Miloh (1982) obtained

https://doi.org/10.1017/jfm.2018.322 Published online by Cambridge University Press

a finite leading-order solution at $\tau = 1/4$ by accounting for cubic self-interactions of resonant waves under the assumption of weak nonlinearity. It was found that the inclusion of (third-order) cubic self-interactions slightly corrects the wavenumbers (for a given frequency) and thus the group velocities of resonant wave modes, leading to the suppression of wave resonance. Zhang & Zhu (1995) used the nonlinear point-source solution of Dagan & Miloh (1982) as a Green function to construct a quasi-linear solution in terms of a source distribution on the body. With the strength of the source determined from the body boundary condition only, the quasi-linear solution does not contain the full nonlinear free-surface effect due to third-order self-interactions in the presence of a body. The feature of the nonlinear seakeeping solution for a body in the neighbourhood of $\tau = 1/4$ remains unknown.

The primary interest of this work is to investigate theoretically and numerically the dominant nonlinear effect upon the seakeeping solution for a body in the neighbourhood of the critical frequency. In an asymptotic analysis near $\tau = 1/4$, we follow Dagan & Miloh (1982) to take into account the cubic self-interactions of resonant waves in the free-surface boundary condition (§ 2), which provide the leading-order nonlinear correction to the linear dispersion relation. Based on the source method, we construct the nonlinear solution for a body in terms of the source distributed on the body surface, with the unknown source strength determined such that both the nonlinear free surface boundary condition and the body boundary condition are satisfied. The detailed derivation and analysis of the nonlinear solution is provided for the case of a 2D submerged body (§§ 3.1 and 3.3). An approximate solution of the nonlinear correction to the wavenumbers of resonant wave modes near $\tau = 1/4$ for a deeply submerged body is derived in terms of the body forcing function and a body geometry parameter Γ (Liu & Yue 1993). The extension of the theoretical analysis to a 3D submerged body is outlined (§ 3.4). We find that for a 2D or 3D body with non-zero volume (for which $\Gamma \neq 0$), the dominant nonlinear correction to the (finite) linear solution due to cubic self-interactions of resonant waves in the neighbourhood of $\tau = 1/4$ is of the first order in the body motion amplitude (or the wave steepness), which is of the same order as the linear solution. Because of the nonlinear effect in the dispersion relation, the wavenumbers of the two resonant wave modes become complex-valued so that they become evanescent (at $\tau < 1/4$ near the critical frequency), with their amplitudes vanishing far upstream and downstream of the body. When the body shrinks to a point (for which $\Gamma = 0$), the present solution reduces to that of a point source, which is consistent with Dagan & Miloh (1982).

To assist in understanding the theoretical analysis, we apply the theory to the special case of a 2D submerged circular cylinder, for which we derive the closed-form solution for the (spatial) damping coefficients of the resonant waves in the neighbourhood of $\tau = 1/4$. Direct numerical simulation of the original nonlinear radiation problem in the time domain for the circular cylinder, based on the high-order spectral method for nonlinear wave–body interactions (Liu, Dommermuth & Yue 1992), is performed to verify the theory (§ 4). The theoretical prediction of the spatial damping rate of the resonant waves and the first-order nonlinear corrections to the linear added mass and wave damping coefficients of the body are all confirmed by the numerical simulation. Since the extension of the theoretical analysis to a surface-piercing body is challenging, we perform fully nonlinear time-domain simulation of the radiation problem for a 3D ship hull, based on the mixed Euler–Lagrangian approach with a quadratic boundary-element method (Liu, Xue & Yue 2001; Yan & Liu 2011) (§ 5). Similar nonlinear solution behaviours to submerged bodies in the neighbourhood of the critical frequency $\tau = 1/4$ are obtained for surface-piercing bodies.

https://doi.org/10.1017/jfm.2018.322 Published online by Cambridge University Press

For clarity, we remark that the present work is motivated by the conclusion of Dagan & Miloh (1982) for a point source. It is a generalization of the work of Dagan & Miloh (1982) to a body for which a source distribution on the body surface is needed. Importantly, the effect of the cubic self-interactions of resonant waves on the solution for a body is found to be characteristically different from that for a point source. In the case of a 2D (or 3D) point source of strength $O(\epsilon)$, the classical linear solution is singular at the critical frequency; and Dagan & Miloh (1982) showed that inclusion of the cubic self-interactions of resonant waves is necessary to cancel the singularity at the critical frequency, leading to a regular solution of $O(\epsilon^{1/2})$ (or $\epsilon \ln \epsilon$). In the case of a 2D or 3D body (with $\Gamma \neq 0$) with a motion amplitude of $O(\epsilon)$, the linear problem itself is regular and has a solution of $O(\epsilon)$. The contribution from the cubic self-interactions is shown to also be $O(\epsilon)$, which is the same order of magnitude as the linear solution. This theoretical result is further verified by direct numerical simulations that solve the original nonlinear initial boundary-value problem. This behaviour of the solution for a body distinctively differs from that for a single point source. In the case of the body, the dominant effect of the cubic self-interactions on the resonant waves is found to add spatial damping to these waves, which was not found for a point source by Dagan & Miloh (1982). We draw our conclusions in § 6.

2. Formulation of the boundary-value problem

We consider the generalized Kelvin–Neumann problem (Haskind 1954) of a body translating with constant forward speed U parallel to the undisturbed free surface in deep water while at the same time undergoing small oscillatory motion and/or encountering small-amplitude waves at frequency ω. A Cartesian coordinate system o–xyz is chosen to be fixed with the mean position of the body, with the origin located on the mean free surface, x pointing in the direction of forward speed and z positive upwards. We assume that the fluid is inviscid and incompressible, and the motion is irrotational. The total velocity potential $\tilde{\Phi}(x, y, z, t)$ describing the flow contains steady and unsteady components,

$$\tilde{\Phi}(x, y, z, t) = \bar{\phi}(x, y, z) + \Phi(x, y, z, t) = \bar{\phi}(x, y, z) + \mathrm{Re}\{\phi(x, y, z)\mathrm{e}^{\mathrm{i}\omega t}\}, \tag{2.1}$$

where $\bar{\phi}$ is due to the steady forward motion of the body and Φ is associated with the body oscillations and/or incident waves. We focus on the unsteady potential Φ with time harmonic dependence at frequency ω and do not further concern ourselves with $\bar{\phi}$ which is related to the steady wave resistance problem. The primary focus of this work is on the solution of the unsteady problem in the neighbourhood of the critical frequency with $\delta = \sqrt{1 - 4\tau} \ll 1$, where $\tau \equiv U\omega/g$. For non-dimensionalization, we use U and U^2/g as velocity and length scales respectively. We consider the weakly nonlinear problem and use a small parameter ϵ as a measure of the amplitude of oscillatory body motion and/or ambient waves.

The amplitude of the time harmonic potential ϕ in (2.1) satisfies Laplace's equation in the fluid,

$$\nabla^2\phi = 0 \quad z \leqslant 0. \tag{2.2}$$

Under the assumption of weak nonlinearity, ϕ satisfies the nonlinear boundary condition on the mean free surface $z = 0$,

$$-\tau^2\phi - 2\mathrm{i}\tau\frac{\partial\phi}{\partial x} + \frac{\partial^2\phi}{\partial x^2} + \frac{\partial\phi}{\partial z} + \frac{1}{8}\nabla\phi\cdot\nabla(\nabla\phi\cdot\nabla\phi^*) + \frac{1}{8}\nabla\phi\cdot\nabla(\nabla\phi^*\cdot\nabla\phi) + \frac{1}{8}\nabla\phi^*\cdot\nabla(\nabla\phi\cdot\nabla\phi) = 0 \quad \text{on } z = 0, \tag{2.3}$$

https://doi.org/10.1017/jfm.2018.322 Published online by Cambridge University Press

where the superscript $*$ represents the complex conjugate. On the body surface, ϕ satisfies the linearized kinematic condition

$$\frac{\partial \phi}{\partial n} = f(x, y, z) \quad \text{on } \bar{S}_B, \tag{2.4}$$

where $\boldsymbol{n} = (n_x, n_y, n_z)$ is the unit normal out of the body and $\bar{S}_B$ is the mean position of the wetted body surface. In (2.4), the forcing term $f(x, y, z) = O(\epsilon)$ is given in terms of the imposed body oscillation and/or incident waves as well as the so-called 'm-terms' due to the steady potential $\bar{\phi}$ (Newman 1978). In deep water, the unsteady fluid velocity vanishes,

$$\nabla \phi \to 0 \quad \text{as } z \to -\infty. \tag{2.5}$$

The boundary-value problem for ϕ is complete with the imposition of an appropriate radiation condition, in this case a physical requirement that only a wave with group velocity greater (less) than the forward speed can be present far up- (down)stream of the body.

In (2.3), the cubic terms represent the leading-order nonlinear effect due to self-interactions of primary harmonic waves at frequency ω, which affects the dispersion relation of the primary waves. The classic linear problem, in which these cubic terms are omitted in (2.3), gives a singular solution of ϕ as $\epsilon\delta^{-1}$ (or $\epsilon \ln \delta$) for a point 2D (or 3D) source/dipole of strength $O(\epsilon)$ at the critical frequency $\tau = 1/4$ (corresponding to $\delta = 0$). Based on the regular perturbation expansion, Dagan & Miloh (1982) showed that the classical linear solution is not uniformly convergent with the perturbation order as $\delta \to 0$. By including the cubic self-interaction terms in the free-surface boundary condition, as in (2.3), they obtained the regular leading-order solution of $O(\epsilon^{1/2})$ (or $O(\epsilon \ln \epsilon)$) for a 2D (or 3D) point source/dipole as $\delta \to 0$. They also showed that this leading-order solution is uniformly convergent with the perturbation order as $\delta \to 0$. The results of Dagan & Miloh (1982) are valid under the assumption of weak nonlinearity since the derivation is based on the regular perturbation expansion.

The purpose of the present study is to understand the importance and behaviours of such nonlinear effects on ϕ in the neighbourhood of the critical frequency in the presence of a body. The only difference in the boundary-value problems of a point source and a body is that the point-source problem does not contain the body boundary condition (2.4). The requirement of satisfying the body boundary condition leads to a solution for a body characteristically different from that for a point source in the neighbourhood of the critical frequency for the linear problem (Liu & Yue 1993). As shown in this work (cf. §§ 3.3 and 3.4), the nonlinear solution (including the effect of cubic self-interaction terms in (2.3)) for a body also characteristically differs from that of Dagan & Miloh (1982) for a point source in the neighbourhood of the critical frequency. The present analysis for a body follows the principles and assumptions of Dagan & Miloh (1982) for a point source, but requires the satisfaction of the body boundary condition (2.4). It is also valid for weakly nonlinear problems only.

One notes that the linearized body boundary condition (2.4) is here considered for simplicity since inclusion of the correction from the nonlinear body boundary effect does not alter the characteristic behaviour of the solution of the problem near the critical frequency. The higher harmonics due to quadratic and other higher-order interactions are not considered here since their frequencies are away from the critical frequency.

To solve the boundary-value problem for ϕ, we construct the solution of ϕ for the general body in terms of a source distribution method (e.g. Brard 1972). We express

https://doi.org/10.1017/jfm.2018.322 Published online by Cambridge University Press

ϕ as the sum of two parts,

$$\phi(x, y, z) = \mathcal{X}(x, y, z) + h(x, y, z), \tag{2.6}$$

where $\mathcal{X}(x, y, z)$ is the potential due to a simple Rankine source distributed on the body surface $\bar{S}_B$ and $h(x, y, z)$ represents the surface wave effect (including free and evanescent waves). Substitution of (2.6) into (2.2), (2.3), (2.4) and (2.5) gives the boundary-value problem for $h(x, y, z)$ in terms of $\mathcal{X}(x, y, z)$,

$$\nabla^2 h = 0, \quad z \leqslant 0, \tag{2.7}$$

$$\left(\mathrm{i}\tau - \frac{\partial}{\partial x}\right)^2 h + \frac{\partial h}{\partial z} + \frac{1}{8}\nabla h^* \cdot \nabla(\nabla h \cdot \nabla h) + \frac{1}{8}\nabla h \cdot \nabla(\nabla h^* \cdot \nabla h) + \frac{1}{8}\nabla h \cdot \nabla(\nabla h \cdot \nabla h^*) = P(x, y) \quad \text{on } z = 0, \tag{2.8}$$

$$\frac{\partial h}{\partial n} = f(x, y, z) - \frac{\partial \mathcal{X}}{\partial n} \quad \text{on } \bar{S}_B, \tag{2.9}$$

$$\nabla h \to 0 \quad \text{as } z \to -\infty. \tag{2.10}$$

In (2.8), the forcing term $P(x, y)$ takes the form

$$P(x, y) = \left[-\left(\mathrm{i}\tau - \frac{\partial}{\partial x}\right)^2 \mathcal{X} - \mathcal{X}_z\right]_{z=0}. \tag{2.11}$$

Equations (2.7)–(2.10) together with the radiation condition form a complete boundary-value problem for $h(x, y, z)$ in terms of $\mathcal{X}(x, y, z)$. One notes that the cubic terms involving cross-products of h and $\mathcal{X}$ from substitution of (2.6) into (2.3) are omitted in (2.8) since these terms are of higher order in δ compared with the self-interaction terms of h which are retained.

In the case of a point source/dipole, $\mathcal{X}(x, y, z)$ is prescribed and $h(x, y, z)$ is directly determined by solving the above boundary-value problem (without the body boundary condition (2.9)). In the case of a body, $h(x, y, z)$ and $\mathcal{X}(x, y, z)$ are coupled through the body boundary condition (2.9). Determination and analysis of their asymptotic solutions near the critical frequency is the main focus of the present work.

3. Theoretical analysis

3.1. *Solution of $h(x, z)$ for given $\mathcal{X}(x, z)$*

For given $\mathcal{X}$, h can be directly determined from the boundary-value problem consisting of (2.7), (2.8), (2.10) and the radiation condition by the use of a Fourier transform. As an illustration and for simplicity, we first consider the 2D problem (in the x–z plane) which was solved by Dagan & Miloh (1982) in the case of a point source. Their key solution procedure is included here to assist in understanding the analysis in the case of a body (cf. § 3.3).

We write the solution of $h(x, z)$ in the form

$$h(x, z) = \frac{1}{\sqrt{2\pi}} \int_{-\infty}^{\infty} \tilde{h}(k) \mathrm{e}^{-\mathrm{i}kx} \mathrm{e}^{|k|z} \, \mathrm{d}k, \quad z \leqslant 0, \tag{3.1}$$

https://doi.org/10.1017/jfm.2018.322 Published online by Cambridge University Press

where $\tilde{h}(k)$ is the Fourier transform of $h(x, z=0)$,

$$\tilde{h}(k) = \frac{1}{\sqrt{2\pi}} \int_{-\infty}^{\infty} h(x, 0) \mathrm{e}^{\mathrm{i}kx} \, \mathrm{d}x. \tag{3.2}$$

For clarity in later reference, we denote the Fourier transform of $h^*(x, z)$ by

$$\tilde{h}^\star(k) = \frac{1}{\sqrt{2\pi}} \int_{-\infty}^{\infty} h^*(x, 0) \mathrm{e}^{\mathrm{i}kx} \, \mathrm{d}x. \tag{3.3}$$

Here, $h(x, z)$ in (3.1) satisfies Laplace's equation (2.7) and the deep water condition (2.10). The unknown function $\tilde{h}(k)$ can be found from the free-surface boundary condition (2.8) together with the radiation condition.

Upon taking the Fourier transform of (2.8), we have

$$\begin{aligned} &\frac{1}{8} \int_{-\infty}^{\infty} \nabla h^* \cdot \nabla (\nabla h \cdot \nabla h) \mathrm{e}^{\mathrm{i}kx} \, \mathrm{d}x + \frac{1}{8} \int_{-\infty}^{\infty} \nabla h \cdot \nabla (\nabla h^* \cdot \nabla h) \mathrm{e}^{\mathrm{i}kx} \, \mathrm{d}x \\ &\quad + \frac{1}{8} \int_{-\infty}^{\infty} \nabla h \cdot \nabla (\nabla h^* \cdot \nabla h) \mathrm{e}^{\mathrm{i}kx} \, \mathrm{d}x + A(\tau, k) \tilde{h}(k) = \tilde{P}(k) \quad \text{on } z = 0, \end{aligned} \tag{3.4}$$

where

$$\tilde{P}(k) = \frac{1}{\sqrt{2\pi}} \int_{-\infty}^{\infty} P(x) \mathrm{e}^{\mathrm{i}kx} \, \mathrm{d}x \tag{3.5}$$

and

$$A(\tau, k) \equiv -\tau^2 - 2\tau k + |k| - k^2. \tag{3.6}$$

By making use of the Faltung theorem (e.g. Dagan & Miloh 1980, 1982; Bracewell 1986) for the cubic terms on the left-hand side in (3.4), we obtain

$$A(\tau, k) \tilde{h}(k) - \frac{1}{4} \int_{-\infty}^{\infty} \int_{-\infty}^{\infty} a(k, \nu, \lambda) \tilde{h}(\nu) \tilde{h}(\lambda - \nu) \tilde{h}^\star(k - \lambda) \, \mathrm{d}\nu \, \mathrm{d}\lambda = \tilde{P}(k), \tag{3.7}$$

where

$$\begin{aligned} a(k, \nu, \lambda) \;=\; &\frac{1}{\pi} \Big\{ (\tau + \nu)[|\lambda - \nu| + |k - \lambda|](k - \lambda) \, [(\lambda - \nu)(k - \lambda) \\ &- |\lambda - \nu||k - \lambda| \,] - (k - \lambda - \tau) \, [\, 2\tau\lambda^2 |\lambda - \nu| - 2\tau\nu|\nu|(\lambda - \nu) \\ &+ |\nu|(\nu - |\nu|)(\lambda - \nu)(|\lambda - \nu| + |\nu|) \,] - \Big[(\lambda - \nu)\nu^2 (k - \lambda) \\ &+ \frac{1}{2}(\lambda - \nu)\nu(k - \lambda)^2 - |\lambda - \nu||\nu|(k - \lambda)\nu - (\lambda - \nu)|\nu||k - \lambda|\nu \\ &- (\lambda - \nu)|\nu|(k - \lambda)|k - \lambda| + |\lambda - \nu|\nu^2 |k - \lambda| + \frac{1}{2}|\lambda - \nu||\nu|(k - \lambda)^2 \Big] \Big\}. \end{aligned} \tag{3.8}$$

https://doi.org/10.1017/jfm.2018.322 Published online by Cambridge University Press

From (3.7), we obtain the solution of $\tilde{h}(k)$, which can be expressed in a form similar to the linear solution,

$$\tilde{h}(k) = \frac{\tilde{P}(k)}{A_g(\tau, k)}, \tag{3.9}$$

with

$$A_g(\tau, k) = A(\tau, k) + d(\tau, k, f), \tag{3.10}$$

where d is an unknown function representing the leading-order nonlinear effect in the dispersion relation, which depends on τ and the body forcing f. Following the derivation of the linear solution, we further express $A_g(\tau, k)$ as

$$A_g(\tau, k) = -(k - k_{1g})(k - k_{2g}) \quad (k > 0), \tag{3.11}$$

$$A_g(\tau, k) = -(k - k_3)(k - k_4) \quad (k < 0), \tag{3.12}$$

where k_{1g} and k_{2g} are given by the roots of the nonlinear dispersion relation of $A_g(\tau, k) = 0$,

$$k_{1g} = \tfrac{1}{2}(1 - 2\tau + \sqrt{\delta^2 + 4d}), \quad k_{2g} = \tfrac{1}{2}(1 - 2\tau - \sqrt{\delta^2 + 4d}), \tag{3.13a,b}$$

which are the wavenumbers of the two resonant wave modes as $\delta \to 0$. Here, k_3 and k_4 are the wavenumbers of the non-resonance waves, given by

$$k_3 = \tfrac{1}{2}(-1 - 2\tau + \sqrt{1 + 4\tau}), \quad k_4 = \tfrac{1}{2}(-1 - 2\tau - \sqrt{1 + 4\tau}). \tag{3.14a,b}$$

On substituting $\tilde{h}(k)$ in (3.9) into (3.1) and splitting the integral with k into two parts, we have

$$\begin{aligned} h(x, z) \;=\; & -\frac{1}{\sqrt{2\pi}\sqrt{\delta^2 + 4d}} \int_0^\infty \left(\frac{1}{k - k_{1g}} - \frac{1}{k - k_{2g}} \right) \tilde{P}(k) \mathrm{e}^{-\mathrm{i}kx} \mathrm{e}^{|k|z} \, \mathrm{d}k \\ & + \frac{1}{\sqrt{2\pi}} \int_{-\infty}^0 \frac{\tilde{P}(k)}{A_g(\tau, k)} \mathrm{e}^{-\mathrm{i}kx} \mathrm{e}^{|k|z} \, \mathrm{d}k. \end{aligned} \tag{3.15}$$

Here, both k_{1g} and k_{2g} have positive real parts. In the limit of linear solution (with $d = 0$), k_{1g} and k_{2g} reduce to $k_{1,2} = (1 - 2\tau \pm \delta)/2$ (e.g. Liu & Yue 1993). At the critical frequency ($\delta = 0$), $k_{1g,2g} = k_c \pm d^{1/2}$, where the critical wavenumber $k_c = 1/4$.

By applying contour integration for the first integral in (3.15) by the use of the indented contours shown in figure 1 and with the imposition of the radiation condition, we obtain

$$\begin{aligned} h(x, z) \;=\; & -\frac{\mathrm{i}\sqrt{2\pi}}{\sqrt{\delta^2 + 4d}} \tilde{P}(k_{2g}) \mathrm{e}^{-\mathrm{i}k_{2g}x + |k_{2g}|z} \\ & - \frac{\mathrm{i}}{\sqrt{2\pi}} \int_0^\infty \frac{\tilde{P}(-\mathrm{i}k)}{A(\tau, -\mathrm{i}k) + d} \mathrm{e}^{-kx + |k|z} \, \mathrm{d}k + \frac{1}{\sqrt{2\pi}} \int_{-\infty}^0 \frac{\tilde{P}(k)}{A(\tau, k) + d} \mathrm{e}^{-\mathrm{i}kx + |k|z} \, \mathrm{d}k \end{aligned} \tag{3.16}$$

https://doi.org/10.1017/jfm.2018.322 Published online by Cambridge University Press

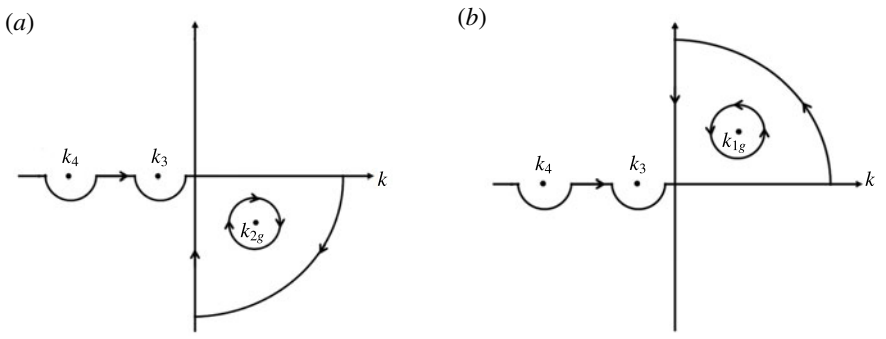


FIGURE 1. Sketch of the indented contours and locations of the poles at $k = k_{1g}$ and k_{2g} in the complex k-plane for integrals in (3.15) for (*a*) $x > 0$ and (*b*) $x < 0$.

for $x > 0$ and

$$h(x, z) = -\frac{\mathrm{i}\sqrt{2\pi}}{\sqrt{\delta^2 + 4d}}\tilde{P}(k_{1g})\mathrm{e}^{-\mathrm{i}k_{1g}x + |k_{1g}|z} + \frac{\mathrm{i}}{\sqrt{2\pi}}\int_0^\infty \frac{\tilde{P}(\mathrm{i}k)}{A(\tau, \mathrm{i}k) + d}\mathrm{e}^{kx+|k|z}\,\mathrm{d}k + \frac{1}{\sqrt{2\pi}}\int_{-\infty}^0 \frac{\tilde{P}(k)}{A(\tau, k) + d}\mathrm{e}^{-\mathrm{i}kx+|k|z}\,\mathrm{d}k \tag{3.17}$$

for $x < 0$. Near the critical frequency, the solution of $h(x, z)$ is dominated by the first term in (3.16) (or (3.17)) for $x > 0$ (or $x < 0$), which is $O(\epsilon\delta^{-1})$, while the other terms in (3.16) (or (3.17)) are $O(\epsilon)$ in the limit of $d = 0$.

To find the unknown function d, we substitute $\tilde{h}(k)$ in (3.9) into (3.7) and carry out the double integration via contour integration. Upon retaining the leading-order (in δ) contributions due to the residues of the poles of the integrand in the complex ν- and λ-planes, we have

$$A(\tau, k)\frac{\tilde{P}(k)}{A_g(\tau, k)} - \pi^2\frac{a(-k_c, k_c, k_c)\tilde{P}^\star(-k_c)\tilde{P}(k_c)\tilde{P}(k_c)}{(\delta^2 + 4d)A_g(\tau, k)} = \tilde{P}(k), \tag{3.18}$$

where $\tilde{P}^\star$ is the Fourier transform of $P^*(x)$ (cf. (3.3)). From the definition of $\tilde{P}^\star$ (cf. (3.3)) and (3.5), it follows that $\tilde{P}^\star(-k_c) = \tilde{P}^*(k_c)$. From (3.8), we have $a(-k_c, k_c, k_c) = -2k_c^4/\pi$. By substituting $a(-k_c, k_c, k_c)$ into (3.18) and letting $k = k_c$, we obtain

$$A(\tau, k) + \frac{2\pi k_c^4\tilde{P}^\star(-k_c)\tilde{P}(k_c)}{(\delta^2 + 4d)} = A_g(\tau, k), \tag{3.19}$$

from which we then obtain the equation to determine d in the neighbourhood of the critical frequency,

$$(\delta^2 + 4d)d = 2\pi k_c^4|\tilde{P}(k_c)|^2. \tag{3.20}$$

https://doi.org/10.1017/jfm.2018.322 Published online by Cambridge University Press

3.2. *Solution for a two-dimensional point source*

For a two-dimensional point source located at $(0, -H)$ with strength characterized by a small dimensionless parameter ϵ, $\mathcal{X}$ is given by

$$\mathcal{X}(x, z) = \frac{\epsilon}{\pi} \ln\left(\frac{r}{r_1}\right), \tag{3.21}$$

where $r = \sqrt{x^2 + (z+H)^2}$ and $r_1 = \sqrt{x^2 + (z-H)^2}$. From (2.11), $P(x)$ is determined as

$$P(x) = -\mathcal{X}_z(x, 0) = \frac{2\epsilon H}{\pi(x^2 + H^2)}. \tag{3.22}$$

Then, we obtain $\tilde{P}(k)$ from (3.5) using (3.22),

$$\tilde{P}(k) = 2\epsilon \frac{\mathrm{i}k}{\sqrt{2\pi}} \mathrm{e}^{-|k|H}. \tag{3.23}$$

From (3.20), d is determined as

$$d = \pm \frac{\epsilon}{2^6} \mathrm{e}^{-k_c H}. \tag{3.24}$$

The positive solution of d is consistent with Dagan & Miloh (1982) while the negative solution of d is chosen to be omitted in Dagan & Miloh (1982). Substitution of d in (3.24) into (3.16) and (3.17) leads to $h(x, z) = O(\epsilon^{1/2})$ in the neighbourhood of the critical frequency (as $\delta \to 0$).

3.3. *Solution for a two-dimensional body*

In the case of a body, $\mathcal{X}$ is unknown *a priori* and it is coupled with h by the body boundary condition (2.9). The potential $\mathcal{X}$ needs to be solved together with h by satisfying the free-surface boundary condition (2.8) and the body boundary condition (2.9).

For a two-dimensional submerged body, we express $\mathcal{X}(x, z)$ in the form

$$\mathcal{X}(x, z) = \int_{\bar{S}_B} \sigma(s') \ln(r/r_1)\, \mathrm{d}s', \tag{3.25}$$

where

$$r = \sqrt{(x-x')^2 + (z-z')^2}, \quad r_1 = \sqrt{(x-x')^2 + (z+z')^2} \tag{3.26a,b}$$

and $\sigma(s')$ represents the unknown strength of the source distributed on the body surface. Here, we use $s = (x, z)$ to represent the field point where the potential is calculated while we use $s' = (x', z')$ to represent the location of the source. Substitution of (3.25) into (2.11) yields

$$P(x) = -2 \int_{\bar{S}_B} \sigma(s') \left(\frac{\partial}{\partial z} \ln r\right)_{z=0} \mathrm{d}s'. \tag{3.27}$$

https://doi.org/10.1017/jfm.2018.322 Published online by Cambridge University Press

By using the identity

$$\ln r = \int_0^\infty \frac{\mathrm{e}^{-k} - \mathrm{e}^{-k|z-z'|}\cos k(x-x')}{k}\,\mathrm{d}k, \tag{3.28}$$

we can rewrite (3.27) as

$$P(x) = -\int_{-\infty}^{\infty} \mathrm{e}^{-\mathrm{i}kx}\left\{\int_{\bar{S}_B} \mathrm{e}^{|k|z'}\mathrm{e}^{\mathrm{i}kx'}\sigma(s')\,\mathrm{d}s'\right\}\mathrm{d}k, \tag{3.29}$$

which corresponds to

$$\tilde{P}(k) = -\sqrt{2\pi}\int_{\bar{S}_B} \mathrm{e}^{|k|z'}\mathrm{e}^{\mathrm{i}kx'}\sigma(s')\,\mathrm{d}s'. \tag{3.30}$$

On substituting $h(x,z)$ in (3.16) and (3.17) as well as $\mathcal{X}(x,z)$ in (3.25) into the body boundary condition (2.9), we have

$$\begin{aligned}
&\pi\sigma(s) + \bar{\mathcal{X}}_n(s) - \frac{\mathrm{i}\sqrt{2\pi}}{\sqrt{\delta^2+4d}}(-\mathrm{i}k_{2g}n_x + |k_{2g}|n_z)\tilde{P}(k_{2g})\mathrm{e}^{-\mathrm{i}k_{2g}x+|k_{2g}|z} \\
&\quad - \frac{\mathrm{i}}{\sqrt{2\pi}}\int_0^\infty \left\{\frac{(-kn_x+|k|n_z)\tilde{P}(-\mathrm{i}k)}{A(\tau,-\mathrm{i}k)+d}\mathrm{e}^{-kx+|k|z}\right\}\mathrm{d}k \\
&\quad + \frac{1}{\sqrt{2\pi}}\int_{-\infty}^0 \left\{\frac{(-\mathrm{i}kn_x+|k|n_z)\tilde{P}(k)}{A(\tau,k)+d}\mathrm{e}^{-\mathrm{i}kx+|k|z}\right\}\mathrm{d}k = f(s), \quad s(x>0)\in\bar{S}_B
\end{aligned} \tag{3.31}$$

and

$$\begin{aligned}
&\pi\sigma(s) + \bar{\mathcal{X}}_n(s) - \frac{\mathrm{i}\sqrt{2\pi}}{\sqrt{\delta^2+4d}}(-\mathrm{i}k_{1g}n_x + |k_{1g}|n_z)\tilde{P}(k_{1g})\mathrm{e}^{-\mathrm{i}k_{1g}x+|k_{1g}|z} \\
&\quad + \frac{\mathrm{i}}{\sqrt{2\pi}}\int_0^\infty \left\{\frac{(kn_x+|k|n_z)\tilde{P}(\mathrm{i}k)}{A(\tau,\mathrm{i}k)+d}\mathrm{e}^{kx+|k|z}\right\}\mathrm{d}k \\
&\quad + \frac{1}{\sqrt{2\pi}}\int_{-\infty}^0 \left\{\frac{(-\mathrm{i}kn_x+|k|n_z)\tilde{P}(k)}{A(\tau,k)+d}\mathrm{e}^{-\mathrm{i}kx+|k|z}\right\}\mathrm{d}k = f(s), \quad s(x<0)\in\bar{S}_B,
\end{aligned} \tag{3.32}$$

where $\bar{\mathcal{X}}_n(s)$ is defined as

$$\bar{\mathcal{X}}_n(s) \equiv \fint_{\bar{S}_B} \sigma(s')\frac{\partial}{\partial n}[\ln(r/r_1)]\,\mathrm{d}s', \tag{3.33}$$

in which the Cauchy principal-value integral is indicated.

To illustrate the characteristic features of the solution near the critical frequency, we here consider the case of a deeply submerged body with centre submergence H. In this case, the two integrals on the left-hand sides of (3.31) and (3.32) behave like $\sim O(\mathrm{e}^{-2kH})$, and they are much smaller than the forcing term $f(s)$, so that they can be neglected in (3.31) and (3.32). Near the critical frequency, $k_{1g,2g} = k_c \pm d^{1/2} \approx k_c$ in weak nonlinearity. Using these facts, (3.31) and (3.32) reduce to the same equation,

$$\pi\sigma(s) + \bar{\mathcal{X}}_n(s) - \frac{\mathrm{i}\sqrt{2\pi}}{\sqrt{\delta^2+4d}}(-\mathrm{i}k_cn_x + k_cn_z)\tilde{P}(k_c)\mathrm{e}^{-\mathrm{i}k_cx+k_cz} = f(s), \quad s\in S_B. \tag{3.34}$$

https://doi.org/10.1017/jfm.2018.322 Published online by Cambridge University Press

By multiplying each side of (3.34) by the term $\mathrm{e}^{\mathrm{i}k_c x+|k_c|z}$ and integrating the equation over the body surface $\bar{S}_B$, we obtain

$$-\pi\tilde{P}(k_c)-\mathrm{i}2\pi\frac{\tilde{P}(k_c)\Gamma k_c}{\sqrt{\delta^2+4d}}=\sqrt{2\pi}\mathcal{F}(k_c), \tag{3.35}$$

where

$$\Gamma(k_c)=\int_{\bar{S}_B}(-\mathrm{i}n_x+n_z)\mathrm{e}^{2k_c z}\,\mathrm{d}s=2k_c\int\int_B \mathrm{e}^{2k_c z}\,\mathrm{d}S \tag{3.36}$$

where B is the mean body section and

$$\mathcal{F}(k_c)=\int_{\bar{S}_B}[f(x,z)-\bar{\mathcal{X}}_n(s)]\mathrm{e}^{\mathrm{i}k_c x+k_c z}\,\mathrm{d}s. \tag{3.37}$$

From (3.35), we obtain $\tilde{P}(k_c)$ in terms of d and $\mathcal{F}(k_c)$,

$$\tilde{P}(k_c)=-\left(\frac{2}{\pi}\right)^{1/2}\frac{\sqrt{\delta^2+4d}}{\sqrt{\delta^2+4d}+\mathrm{i}2k_c\Gamma}\mathcal{F}(k_c). \tag{3.38}$$

Substitution of $\tilde{P}(k_c)$ in (3.38) into (3.34) yields a new integral equation for σ,

$$\pi\sigma(s)+\bar{\mathcal{X}}_n(s)+\frac{2k_c(n_x+\mathrm{i}n_z)\mathcal{F}(k_c)}{\sqrt{\delta^2+4d}+\mathrm{i}2k_c\Gamma}\mathrm{e}^{-\mathrm{i}k_c x+k_c z}=f(s),\quad s\in S_B. \tag{3.39}$$

It follows from (3.39) that for $\Gamma\neq 0$, $\sigma=O(\epsilon)$ (since $\sigma(s)\sim f(s)$) and is bounded as $\delta\to 0$.

Substitution of (3.38) into (3.20) gives the equation to determine d,

$$4d^2+(\delta^2+4k_c^2\Gamma^2)d-4k_c^4|\mathcal{F}(k_c)|^2=0. \tag{3.40}$$

Two solutions for d are obtained as a function of the body forcing f and body geometry parameter Γ,

$$d_{1,2}=-\frac{1}{2}\left(\frac{\delta^2}{4}+k_c^2\Gamma^2\right)\pm\frac{1}{2}\left[\left(\frac{\delta^2}{4}+k_c^2\Gamma^2\right)^2+4k_c^4|\mathcal{F}(k_c)|^2\right]^{1/2}, \tag{3.41}$$

with d_1 (or d_2) corresponding to the plus (or minus) sign in (3.41). Once d is determined, we have $\tilde{P}(k_c)$ from (3.38), $h(x,z)$ from (3.16) and (3.17), and $\mathcal{X}(x,z)$ from (3.25), with $\sigma(s)$ from (3.39).

We see from (3.41) that d_1 is always positive and $d_1=O(\epsilon)$. The wavenumbers of the two resonant wave modes are $k_{1g,2g}=k_c\pm(1/2)(\delta^2+4d_1)^{1/2}$, indicating that $k_{1g}>k_c$ and $k_{2g}<k_c$. The solution d_2 is negative definite, and $d_2=O(1)$ for $\Gamma\neq 0$. The associated wavenumbers $k_{1g,2g}=k_c\pm(1/2)(\delta^2+4d_2)^{1/2}$ become complex as $\delta\to 0$. In this case, $\mathrm{Im}\,k_{1g,2g}=\pm(1/2)\mathrm{Im}(\delta^2+4d_2)^{1/2}$, which is equal to $\pm|d_2|^{1/2}$ at $\delta=0$, representing the spatial damping coefficient of the resonant waves. This solution shows that the two resonant wave modes become evanescent waves near the critical frequency. For $\Gamma=0$, the solution reduces to $d_{1,2}=O(\epsilon)$, consistent with the solution for a point source/dipole (Dagan & Miloh 1982).

https://doi.org/10.1017/jfm.2018.322 Published online by Cambridge University Press

The dominant part of the nonlinear solution of $h(x, z)$ associated with the resonant wave modes can be expressed as

$$h_{NL}(x, z) = \frac{\mathrm{i}2\mathcal{F}(k_c)}{\sqrt{\delta^2 + 4d} + \mathrm{i}2k_c\Gamma} \mathrm{e}^{-\mathrm{i}k_{1g,2g}x + |k_{1g,2g}|z} \tag{3.42}$$

for $x < 0$ and $x > 0$. By setting $d = 0$, equation (3.42) reduces to the linear solution,

$$h_L(x, z) = \frac{\mathrm{i}2\mathcal{F}(k_c)}{\delta + \mathrm{i}2k_c\Gamma} \mathrm{e}^{-\mathrm{i}k_c x + k_c z}, \tag{3.43}$$

which is consistent with that of Liu & Yue (1993). From (3.42) and (3.43), we have $h_{NL} = O(\epsilon)$ and $h_L = O(\epsilon)$ as $\delta \to 0$ if $\Gamma \neq 0$. The difference between the amplitudes of h_{NL} and h_L characterizes the order of magnitude of the nonlinear correction due to the cubic self-interaction effect,

$$h_{COR1}(x, z) = |h_{NL}| - |h_L| \sim \frac{4\mathcal{F}(k_c)\mathrm{e}^{k_c z} d_1}{\delta^2 + 4k_c^2\Gamma^2} \tag{3.44}$$

for $d = d_1$ and

$$h_{COR2}(x, z) = |h_{NL}| - |h_L| \sim \frac{2\mathcal{F}(k_c)\mathrm{e}^{k_c z}(\mathrm{e}^{\pm \nu x} - 1)}{\delta^2 + 4k_c^2\Gamma^2} \tag{3.45}$$

for $x < 0$ and $x > 0$ with $d = d_2$, where the spatial damping factor $\nu = \mathrm{Im}(\delta^2 + 4d_2)^{1/2}/2$. For $\Gamma \neq 0$, $h_{COR1} = O(\epsilon^2)$ while $h_{COR2} = O(\epsilon)$ as $\delta \to 0$. The nonlinear correction h_{COR2}, associated with $d = d_2$, dominates over h_{COR1} associated with $d = d_1$. Importantly, h_{COR2} is of the same order of magnitude as the (leading-order) linear solution h_L. This shows that although the linear solution h_L is bounded (for $\Gamma \neq 0$), h_L is a partial contribution to the leading-order solution. It is necessary to include the cubic nonlinear self-interaction effects in order to obtain the complete leading-order solution near the critical frequency.

If $\Gamma(k_c) = 0$, the solution reduces to that for a point source with $h_L = O(\epsilon/\delta)$ and $h_{NL} = O(\epsilon^{1/2})$ as $\delta \to 0$, which is consistent with Dagan & Miloh (1982).

We note that Γ is always positive definite for a submerged body with non-zero cross-section area (cf. (3.36)). As the cross-section area shrinks to zero, the body becomes like a point and $\Gamma = 0$.

3.4. *Extension to a three-dimensional submerged body*

The foregoing analysis can be generalized to three dimensions. We define the two-dimensional Fourier transform of $h(x, y, z = 0)$ by

$$\tilde{h}(\rho, \theta) = \frac{1}{2\pi} \int_{-\infty}^{\infty} \int_{-\infty}^{\infty} h(x, y, 0)\mathrm{e}^{\mathrm{i}(\rho\cos\theta x + \rho\sin\theta y)}\,\mathrm{d}x\,\mathrm{d}y. \tag{3.46}$$

By making use of the two-dimensional Fourier transform of (2.8), introducing an unknown small parameter d to the dispersion relation for the nonlinear effects and following the same procedure as in § 3.1, we obtain the dominant part of the solution of $h(x, y, z)$ (for given a free surface forcing $P(x, y)$) due to the two resonant wave modes,

$$h(x, y, z) \sim \ln(\delta^2 + d)^{1/2}\tilde{P}(k_c, 0)\mathrm{e}^{-\mathrm{i}k_{1g,2g}x + |k_{1g,2g}z|} \tag{3.47}$$

https://doi.org/10.1017/jfm.2018.322 Published online by Cambridge University Press

as $\delta \to 0$ for $x < 0$ and $x > 0$, where $\tilde{P}(k_c, 0)$ is the two-dimensional Fourier transform of $P(x, y)$ and d is determined from the equation

$$d \sim [\ln(\delta^2 + d)^{1/2}]^2 |\tilde{P}(k_c, 0)|^2. \tag{3.48}$$

In the presence of a submerged three-dimensional body, we follow the same procedure as in § 3.3 to obtain

$$\tilde{P}(k_c, 0) \sim \frac{\mathcal{F}(k_c)}{\pi + \mathrm{i}k_c \Gamma \ln(\delta^2 + d)^{1/2}}, \tag{3.49}$$

where $\Gamma(k_c)$ and $\mathcal{F}(k_c)$ are given by (3.36) and (3.37) but with $\bar{S}_B$ representing the mean surface of the wetted three-dimensional body surface. Upon substituting (3.49) into (3.47) and (3.48), we obtain the dominant part of the solution for $h(x, y, z)$ associated with the two resonant wave modes,

$$h(x, y, z) \sim \frac{\ln(\delta^2 + d)^{1/2}}{\pi + \mathrm{i}k_c \Gamma \ln(\delta^2 + d)^{1/2}} \mathcal{F}(k_c) \mathrm{e}^{-\mathrm{i}k_{1g,2g}x + |k_{1g,2g}z|}, \tag{3.50}$$

and the equation to determine d,

$$d \sim \frac{[\ln(\delta^2 + d)^{1/2}]^2}{\pi^2 + k_c^2 \Gamma^2 [\ln(\delta^2 + d)^{1/2}]^2} |\mathcal{F}(k_c)|^2. \tag{3.51}$$

Two complex-valued roots of d generally exist in (3.51). We see from (3.50) that if $\Gamma \neq 0$, $h_{NL} = O(\epsilon)$ and $h_L = O(\epsilon)$, which follows from (3.50) by setting $d = 0$. The nonlinear correction, due to dominant cubic self-interactions, is $h_{COR} = |h_{NL}| - |h_L| = O(\epsilon)$, since the complex solutions of d give spatial damping effects on the resonant wave modes, which is the same behaviour as in two dimensions. If $\Gamma = 0$, $h_{NL} = O(\epsilon \ln \epsilon)$ while $h_L = O(\epsilon \ln \delta)$ as $\delta \to 0$, consistent with the point-source solution by Dagan & Miloh (1982).

4. Application to a submerged circular cylinder

As an illustration, we consider the special case of a translating and oscillating submerged circular cylinder near $\tau = 1/4$. Following the (frequency-domain) asymptotic analysis in § 3.3, we derive the closed-form theoretical solution of the spatial damping coefficient of the resonant wave modes. To confirm the theory, the numerical solution of the original initial boundary-value problem for the submerged cylinder case is obtained and compared with the theoretical prediction.

4.1. *Analytic solution*

For a submerged circular cylinder with a radius of R and a centre submergence of H, the geometry parameter $\Gamma(k_c) = 2\pi R \mathrm{e}^{-2k_c H} I_1(2k_c R)$, where I_1 is the modified Bessel function of the first kind and $\bar{\mathcal{X}}_n(s) = 0$ (Liu & Yue 1993). The function $\mathcal{F}(k)$ is then given by

$$\mathcal{F}(k) = \int_{\bar{S}_B} f(x, z) \mathrm{e}^{\mathrm{i}kx + kz} \, \mathrm{d}s. \tag{4.1}$$

https://doi.org/10.1017/jfm.2018.322 Published online by Cambridge University Press

For convenience in the calculation of $\mathcal{F}(k)$, we replace (x, z) by the cylindrical coordinates (r, θ). For the radiation problem, we have on the body surface

$$f(R, \theta) = \xi_x \left(\mathrm{i}\tau \cos\theta + \frac{2\cos 2\theta}{R} \right) + \xi_z \left(\mathrm{i}\tau \sin\theta + \frac{2\sin 2\theta}{R} \right), \tag{4.2}$$

where ξ_x and ξ_z are respectively the amplitudes of the surge and heave oscillations. Upon expanding the exponential function in (4.1) in a Taylor series, the integration over θ can be readily carried out to yield

$$\mathcal{F}(k_c) = 2\pi k_c^2 R^2 \mathrm{e}^{-k_c H}(-\xi_x + \mathrm{i}\xi_z). \tag{4.3}$$

Substitution of $\mathcal{F}(k_c)$ in (4.3) into (3.41) gives the solution of d,

$$\begin{aligned} d_2 \;=\; & -\frac{1}{2}\left[\frac{\delta^2}{4} + 4\pi^2 k_c^2 R^2 \mathrm{e}^{-4k_c H} I_1^2(2k_c R) \right] \\ & - \frac{1}{2}\left\{ \left[\frac{\delta^2}{4} + 4\pi^2 k_c^2 R^2 \mathrm{e}^{-4k_c H} I_1^2(2k_c R) \right]^2 + 16 k_c^8 \pi^2 R^4 \mathrm{e}^{-2k_c H}(\xi_x^2 + \xi_z^2) \right\}^{1/2}. \end{aligned} \tag{4.4}$$

The amplitudes of the resonant waves far downstream ($x < 0$) and upstream ($x > 0$) of the body decay with the distance from the body like

$$A_{1,2}(x) \sim \mathrm{e}^{\nu_{1,2} x} \tag{4.5}$$

for $x < 0$ and $x > 0$, with the spatial damping coefficient given by

$$\nu_{1,2} = \pm \tfrac{1}{2} \mathrm{Im}(\delta^2 + 4d_2)^{1/2} \tag{4.6}$$

in the neighbourhood of the critical frequency, with $\delta \ll 1$.

4.2. *Comparison with direct numerical simulation*

To verify the analytical result, we solve the original nonlinear initial boundary-value problem for the submerged circular cylinder in a uniform current by numerical simulation. The comparison of the numerical solution with the analytic prediction provides a verification of the theory.

The simulation is directly performed in the time domain, based on the use of a highly efficient high-order spectral (HOS) method for nonlinear wave–body interactions developed by Liu *et al.* (1992). The time simulation of the nonlinear wave–body interaction problem up to a specified high order M in wave steepness consists of two main steps. Beginning from initial values for the free-surface elevation $\eta(x, t)$ and free-surface potential $\Phi^S(x, t)$, at each successive time step, we (i) solve the nonlinear boundary-value problem to order M based on the perturbation method to obtain the vertical velocity at the free surface and (ii) integrate the evolution equations, which are the nonlinear kinematic and dynamic free-surface boundary conditions, forward for $\eta(x, t + \Delta t)$ and $\Phi^S(x, t + \Delta t)$, where Δt is the time step; the process is then repeated. By use of the Taylor series expansion of $\Phi^S(x, t)$ (on the instantaneous free surface) about the mean free surface, the nonlinear boundary-value problem at each time is expanded into a sequence of linearized boundary-value problems for the perturbed potentials, $\Phi^{(m)}(x, z, t)$, $m = 1, \ldots, M$, which are successively solved by

https://doi.org/10.1017/jfm.2018.322 Published online by Cambridge University Press

the pseudo-spectral method with the use of N_F Fourier spectral modes on the mean free surface and N_B Fourier source modes on the body. With a long-time simulation, we obtain (limited-cycle) steady-state solutions for the surface wave elevation near the body and radiation forces on the body including nonlinear free-surface effects (as in physical laboratory experiments). The harmonic components of the wave elevation and forces on the body are obtained from the steady-state time history via Fourier transform. For more details on the HOS method for nonlinear wave–body simulations, see Liu *et al.* (1992).

We remark that the N_F spectral wave modes and N_B body-source modes are the basis functions used to efficiently represent the solution of each $\Phi^{(m)}(x, z, t)$, $m = 1, \ldots, M$, at this particular time. The amplitudes of these spectral modes are obtained by invoking the boundary conditions that are not automatically satisfied by each spectral mode. For the nonlinear problem, they are not explicitly related to any specific physical wave or body components in general, and their time dependences are unknown *a priori* and may not have any physical meaning.

As demonstrated by Liu *et al.* (1992), by using fast-transform techniques, the operational count per time step is (approximately) linearly proportional to M and N_F (typically $N_F \gg N_B$). For a submerged body, the method obtains the exponential convergence of the solution with respect to M and N_F (for moderately steep waves), and N_B. In the present simulation, we use the length of the periodic computational domain $L_x = 40\lambda_c$, $N_F = 2048$, $N_B = 128$ and time step $\Delta t = T_c/128$, where $\lambda_c = 2\pi/k_c$ and the critical wave period $T_c = 2\pi/\omega_c$. The values of the numerical parameters are determined through convergence tests, with the numerical results unchanged by further varying their values. Simulations with different values of order M are performed to access and quantify the nonlinear free-surface effects. As initial conditions, the free-surface elevation $\eta(x, 0)$ and the potential $\Phi^S(x, 0)$ are prescribed to be zero. To remove possible reflection from the periodic boundaries, we follow Liu *et al.* (1992) to smoothly truncate the free-surface elevation and velocity potential at longitudinal ends of the computational domain after each time step of the simulation.

Figure 2 displays the nonlinear simulation result for the steady-state wave profile above the submerged circular cylinder at the critical frequency $\tau = 1/4$. The nonlinear simulation result (with order $M = 3$) shows that the resonant wave amplitudes downstream ($x < 0$) and upstream ($x > 0$) of the body, $A_{1,2}(x)$, decay with the distance from the body, as predicted by the theory. The analytic solution of the decay rate for the upstream wave amplitude $A_2(x)$ compares well with the numerical solution. Downstream, in addition to the resonant wave whose amplitude $A_1(x)$ decays with $|x|$, two non-resonant propagating waves (with wavenumbers k_3 and k_4) are also present. Unlike upstream of the body, it is difficult to separate the spatially varying amplitude of the resonant wave $A_1(x)$ for a clean comparison with the theoretical prediction downstream of the body.

Figure 3 compares the damping factor of the resonant wave upstream of the body ($A_2(x)$) between the analytic solution (4.6) and nonlinear simulations ($M = 3$) at the critical frequency $\tau = 1/4$ for different body motion amplitudes. At deep submergence ($H/R = 6$), the analytical solution matches well with the nonlinear numerical solution ($M = 3$). Both the analytic solution and the numerical simulation show that the damping factor ν has a weak dependence on the body motion amplitude, as indicated in (4.6). In particular, ν approaches a non-zero asymptote as the body motion amplitude decreases to zero. As the submergence decreases to $H/R = 4$, both the analytic solution and the numerical simulation show the same trend of ν variation with body motion amplitude, but a quantitative discrepancy exists between them since the analytic solution employs the assumption of deep submergence.

https://doi.org/10.1017/jfm.2018.322 Published online by Cambridge University Press

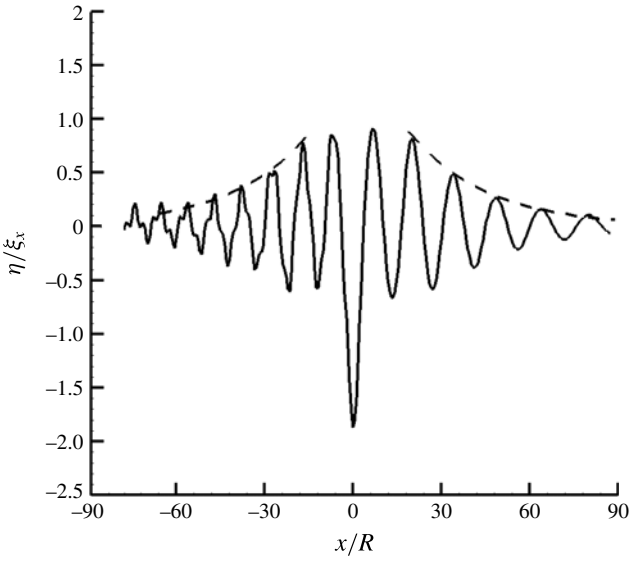


FIGURE 2. Representative instantaneous free-surface shape of the steady-state wave profile above the submerged circular cylinder (with its centre at $x = 0$) obtained by the time-domain nonlinear simulation with $M = 3$ (——). The analytical solutions of the envelope of decaying wave amplitude of resonant waves downstream ($x < 0$) and upstream ($x > 0$) of the body, $A_{1,2}(x) \sim \mathrm{e}^{\pm 0.022x}$, from (4.6) (– – –) are also plotted for comparison. (Here, $H/R = 6$, $F_r = 0.75$, $\tau = 0.25$, $\xi_x/R = 0.05$.)

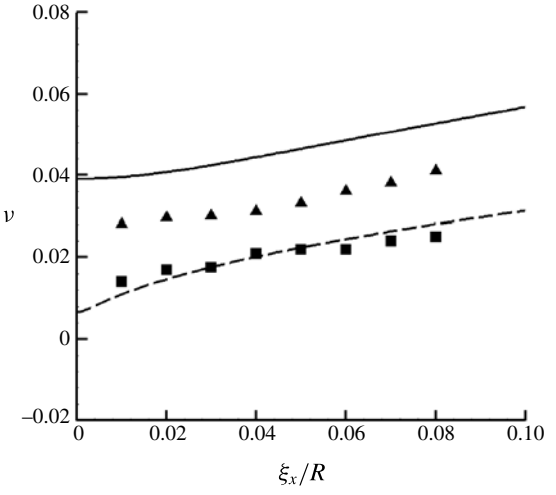


FIGURE 3. Comparison of the damping factor ν_2 of the resonant wave upstream of the body ($A_2(x)$) between the analytic solution from (4.6) with $H/R = 4$ (——) and 6 (– – –), and nonlinear simulations ($M = 3$) with $H/R = 4$ (▲) and 6 (■) as a function of the surge motion amplitude ξ_x/R. (Here, $\tau = 0.25$ and $F_r = 0.75$.)

We compare the theoretical solution of ν_2 with that from nonlinear numerical simulation ($M = 3$) for different body submergences at fixed body motion amplitude.

https://doi.org/10.1017/jfm.2018.322 Published online by Cambridge University Press

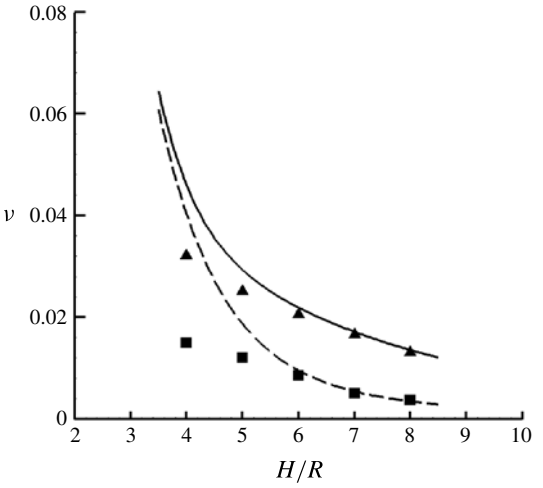


FIGURE 4. Comparison of the damping factor ν_2 of the resonant wave upstream of the body ($A_2(x)$) between the analytic solution from (4.6) at $\tau = 0.245$ (– – –) and 0.25 (——), and nonlinear simulations ($M = 3$) at $\tau = 0.245$ (■) and 0.25 (▲) as a function of body submergence H/R. (Here, $\xi_x/R = 0.05$ and $F_r = 0.75$.)

As shown in figure 4, the agreement between the theoretical solution and the nonlinear simulation is excellent at deep submergence for $\tau = 0.245$ and 0.25. The discrepancy between them increases at shallower submergence, as expected, since the theoretical solution is derived based on the assumption of deep submergence. Additionally, both the theoretical prediction and the numerical simulation show that ν_2 increases with decreasing body submergence. This is consistent with the fact that $d_2 \sim \mathrm{e}^{-kH}$, as shown in (4.4).

The force on the body can be obtained by integration of the pressure over the body in the simulation. The harmonic components can be extracted from the steady-state time history via Fourier transform. The (conventional) added mass and damping coefficients of the body can be determined from the complex amplitude of the first-harmonic force. For example, for surge motion with oscillation $\xi(t) = \xi_x \sin(\omega t)$, the added mass ($A_{xx}$ and A_{zx}) and damping (B_{xx} and B_{zx}) coefficients of the body can be calculated by

$$\left.\begin{aligned} A_{xx} &= 2\,\mathrm{Re}\,F_x/\xi_x\omega^2, \quad A_{zx} = 2\,\mathrm{Re}\,F_z/\xi_x\omega^2, \\ B_{xx} &= -2\,\mathrm{Im}\,F_x/\xi_x\omega, \quad B_{zx} = -2\,\mathrm{Im}\,F_z/\xi_x\omega, \end{aligned}\right\} \tag{4.7}$$

where F_x and F_z are the complex amplitudes of the first-harmonic force on the body in the x- and z-directions respectively.

Figure 5 plots the sample time history of the complex amplitude of the first-harmonic horizontal force on the cylinder at the critical frequency $\tau = 1/4$ with a fixed surge motion amplitude, obtained by numerical simulations with $M = 1$, 2 and 3. The results in the figure show that the nonlinear solution (with $M = 2$, 3) approaches the steady state much faster than the linear solution (with $M = 1$) since the inclusion of nonlinear effects removes the wave resonance. Figure 6 plots the simulation results for the radiation force on the cylinder at the critical frequency $\tau = 1/4$ as a function of the body motion amplitude. The simulation results are

https://doi.org/10.1017/jfm.2018.322 Published online by Cambridge University Press

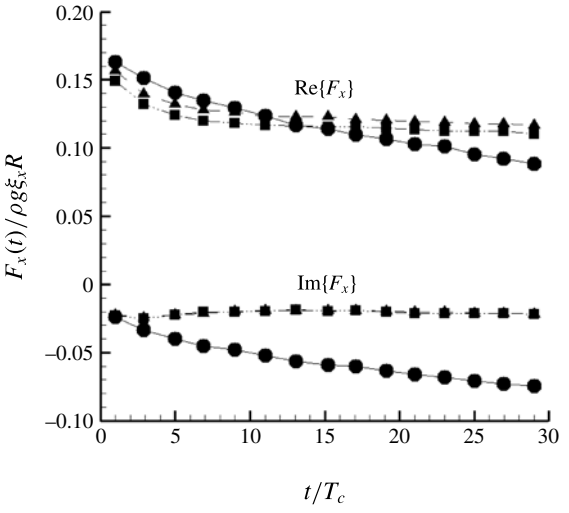


FIGURE 5. Time histories of the real part ($\mathrm{Re}\,F_x$) and imaginary part ($\mathrm{Im}\,F_x$) of the complex amplitude of the first-harmonic radiation force in the horizontal direction on the submerged circular cylinder at $\tau = 0.25$ as a function of simulation time (t/T_c) obtained by numerical simulations with $M = 1$ (●), 2 (▲) and 3 (■). The results for $\mathrm{Im}\,F_x$ with $M = 2$ and 3 overlap each other graphically. (Here, $H/R = 6$, $F_r = 0.75$, $\xi_x/R = 0.05$.)

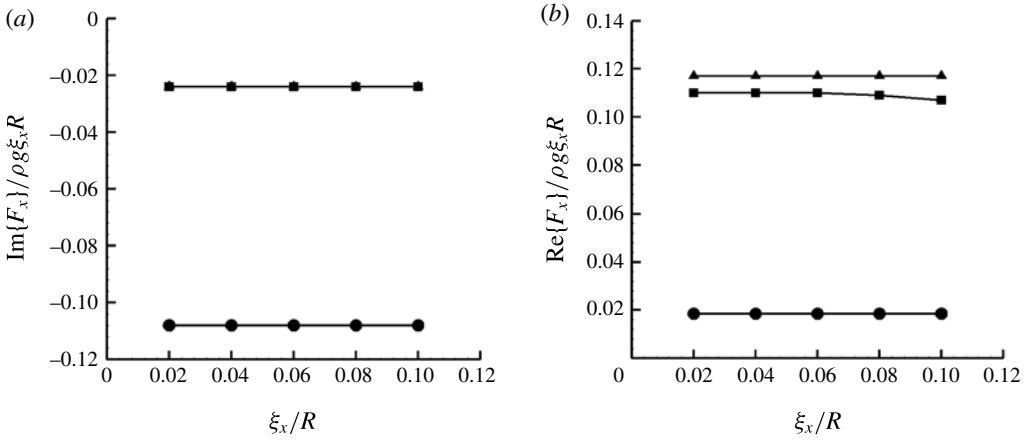


FIGURE 6. The imaginary part (*a*) and real part (*b*) of the radiation force in the horizontal direction on the cylinder at $\tau = 0.25$ as a function of the surge motion amplitude (ξ_x/R) obtained by nonlinear simulations with $M = 1$ (●), 2 (▲) and 3 (■). The results with $M = 2$ and 3 overlap each other graphically. (Here, $H/R = 6$ and $F_r = 0.75$.)

converged with M since the difference between the results with $M = 2$ and 3 is negligibly small. The results with $M = 1$, 2 and 3, normalized by the body motion amplitude, are all nearly constant and independent of the body motion amplitude. This indicates that the linear solution, nonlinear solution and nonlinear correction due to the cubic self-interactions of resonant waves are all of first order in the wave steepness (or body motion amplitude). This confirms the theoretical prediction derived in § 3.3.

https://doi.org/10.1017/jfm.2018.322 Published online by Cambridge University Press

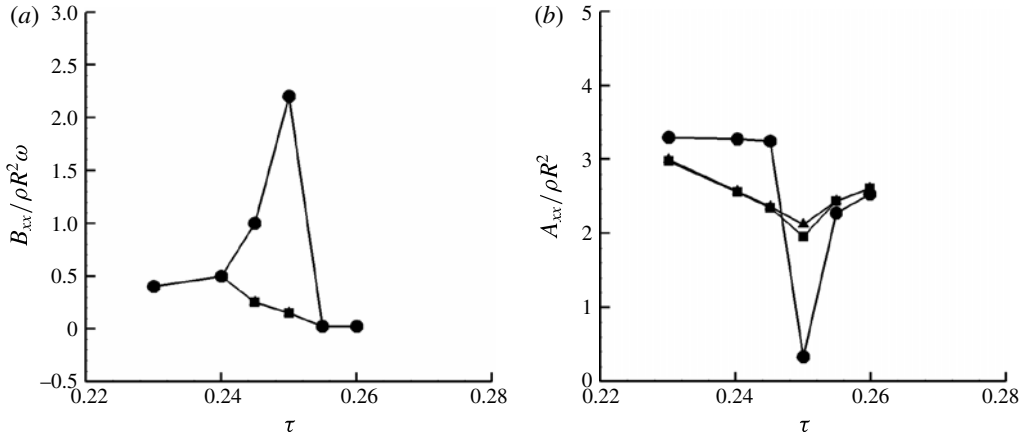


FIGURE 7. The damping coefficient (*a*) and added mass coefficient (*b*) of the submerged circular cylinder in the neighbourhood of $\tau = 0.25$ obtained by nonlinear simulations with $M = 1$ (●), 2 (▲) and 3 (■). The results with $M = 2$ and 3 overlap each other graphically. (Here, $H/R = 6$, $F_r = 0.75$ and $\xi_x/R = 0.05$.)

Figure 7 shows the numerical simulation results with M up to 3 for the wave damping and added mass coefficients of the body in the neighbourhood of $\tau = 1/4$. For both wave damping and added mass, the linear solution ($M = 1$) is finite but varies sharply near $\tau = 1/4$, while the nonlinear solution ($M = 3$) varies smoothly, with the peak value near $\tau = 1/4$ significantly reduced. Such important nonlinear corrections are seen to exist only in a small region near $\tau = 1/4$. For τ away from 1/4, the nonlinear effects become insignificant. The results in figures 6 and 7 indicate that the nonlinear corrections due to the third-order self-interactions should be accounted for in order to obtain the correct prediction of the seakeeping solution near the critical frequency.

The analysis in § 3.3 shows that the behaviour of the solution for a body reduces to that of a point source/dipole in the neighbourhood of $\tau = 1/4$ when the geometry parameter $\Gamma = 0$. For a submerged body, the value of Γ vanishes exponentially with increasing submergence. We thus use the numerical simulation result for a deeply submerged circular cylinder ($H/R = 20$) to check the validity of the theory of Dagan & Miloh (1982) for a point source/dipole, which has not been achieved in the literature. The linear simulation (with $M = 1$) at $\tau = 1/4$ does not reach the steady state, with the solution growing with time indefinitely, indicating that the linear solution is singular in this case. The nonlinear simulation (with $M = 3$) reaches the steady state rapidly. Figure 8 plots the (steady-state) normalized amplitude of the radiated wave (A_2/ξ_x) upstream of the cylinder ($x/R = 80$) at $\tau = 1/4$ as a function of body motion amplitude (ξ_x/R). The nonlinear simulations also show that A_2 does not decay with the distance from the body in this case. The result in figure 8 shows that A_2/ξ_x behaves as $(\xi_x/R)^{-1/2}$, which indicates the nonlinear solution of $A_2 \sim (\xi_x/R)^{1/2} = O(\epsilon^{1/2})$. These numerical results for a deeply submerged body (with $\Gamma \sim 0$) confirm the theory of Dagan & Miloh (1982) for a point source/dipole.

5. Numerical simulation result for a three-dimensional floating body

The theoretical analysis in § 3 is derived for submerged bodies. Extension of the analysis to surface-piercing bodies is not straightforward due to the presence of a

https://doi.org/10.1017/jfm.2018.322 Published online by Cambridge University Press

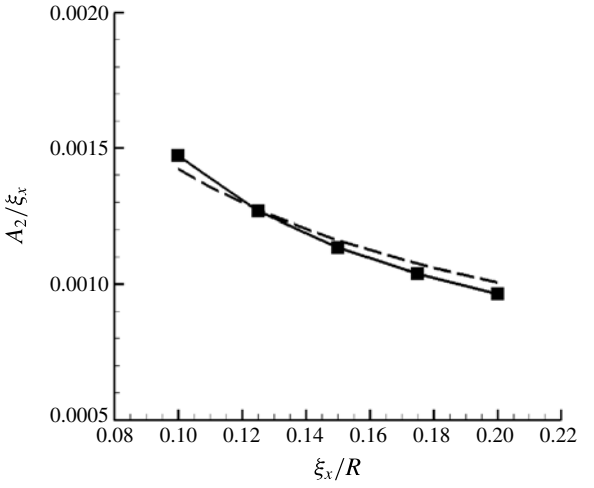


FIGURE 8. The amplitude of the radiated wave upstream of the deeply submerged circular cylinder, A_2/ξ_x, as a function of the surge motion amplitude, ξ_x/R. The plotted results are from nonlinear simulations with $M=3$ (■) and a fitted dependence $(\xi_x/R)^{-1/2}$ (– – –). (Here, $\tau=0.25$, $H/R=20$ and $F_r=0.75$.)

discontinuous free surface. To understand the effect of nonlinear self-interactions of resonant waves on the seakeeping solution near the critical frequency for a surface-piercing body, we apply a time-domain numerical simulation of fully nonlinear wave–body interactions to investigate the heave radiation problem of an advancing ship. The simulation is based on the quadratic boundary-element method with the use of the mixed Euler–Lagrangian (MEL) approach to track the nonlinear free-surface evolution. The simulation accounts for fully nonlinear wave–wave and wave–body interactions and provides a high-fidelity prediction of the nonlinear solution (Liu *et al.* 2001; Yan & Liu 2011; Shen & Liu 2017).

As a numerical example, we consider a Series 60 (S60) ship hull with block coefficient $C_B=0.7$, which is forced to oscillate in the vertical direction at the critical frequency $\tau=1/4$ and Froude number $Fr=U/(gL)^{1/2}=0.2$, where L is the ship length. The numerical parameters used in the simulation are domain size $L_x=L_y=20\lambda_c$, number of free-surface quadratic panels $N_F=20$ per wavelength (λ_c), number of body quadratic panels $N_B=750$ and time step $\Delta t=T_c/100$. A sponge layer is employed in a narrow strip at the outer edge of the computational domain to absorb the radiated waves. The values of the numerical parameters are determined from convergence tests. The use of these numerical parameters ensures that the convergence of the radiation force on the body is within approximately 1 %. Both linear and fully nonlinear simulations are performed to obtain the heave added mass and damping coefficients of the ship hull near the critical frequency.

Figure 9 shows the numerical results for the heave added mass and damping coefficients of the S60 hull at the critical frequency $\tau=1/4$ as a function of the heave motion amplitude ξ_z/L. In figure 9, both the linear and the nonlinear results are normalized by ξ_z/L. Since the normalized results are nearly constant with varying ξ_z/L, the added mass and damping coefficients for a surface-piercing body are nearly linearly dependent on the motion amplitude (or wave steepness). This shows that for a surface-piercing body, the nonlinear correction due to cubic self-interactions in the

https://doi.org/10.1017/jfm.2018.322 Published online by Cambridge University Press

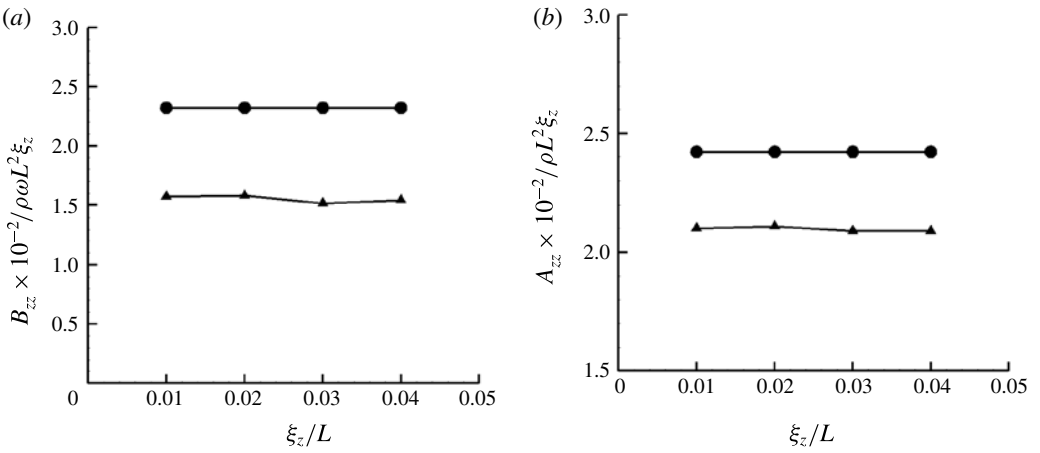


FIGURE 9. The heave damping coefficient (a) and added mass coefficient (b) of a S60 ship hull at the critical frequency $\tau = 0.25$ as a function of the heave motion amplitude ξ_z/L, obtained by linear (●) and fully nonlinear (▲) numerical simulations ($F_r = 0.2$).

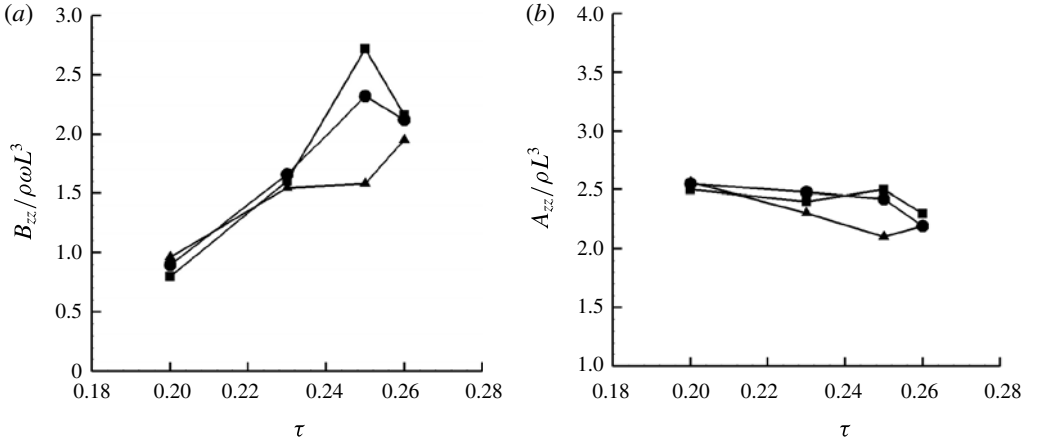


FIGURE 10. The heave damping coefficient (a) and added mass coefficient (b) of a S60 ship hull in the neighbourhood of the critical frequency $\tau = 0.25$ obtained by linear (●) and fully nonlinear (▲) numerical simulations. The linear numerical solution by Bingham (1994) (■) is shown for comparison. (Here, $F_r = 0.2$ and $\xi_z/L = 0.01$.)

neighbourhood of the critical frequency is of the same order of magnitude as the (leading-order) linear solution, as shown theoretically for submerged bodies in § 3.

Figure 10 compares the linear and nonlinear solutions for the added mass and damping coefficients in the neighbourhood of $\tau = 1/4$ for fixed heave motion amplitude $\xi_z/L = 0.01$. The linear numerical result from Bingham (1994), which is based on the constant panel method, is also shown in figure 10 as a validation of our simulations. For both the added mass and the damping coefficients, significant nonlinear corrections are found in the neighbourhood of $\tau = 1/4$. The numerical results in figures 9 and 10 indicate that like submerged bodies, similar important nonlinear effects on the seakeeping solution near the critical frequency exist for surface-piercing bodies.

https://doi.org/10.1017/jfm.2018.322 Published online by Cambridge University Press

6. Conclusion

We have studied theoretically and numerically the nonlinear seakeeping problem of a submerged or floating body in deep water in the neighbourhood of the critical frequency corresponding to $\tau \equiv U\omega/g = 1/4$. For a two-dimensional submerged body, we have shown theoretically that the nonlinear correction to the (finite) linear seakeeping solution due to cubic self-interactions of resonant waves is of the same order of magnitude as the linear solution near $\tau = 1/4$. The resonant waves, which are propagating waves in the linear solution, become evanescent due to the nonlinear effects in the dispersion relation. In the special case of a deeply submerged circular cylinder, we have derived a closed-form analytic solution of the spatial damping coefficient of the resonant waves. The theoretical findings were all confirmed by direct numerical nonlinear simulations in the case of a submerged circular cylinder. We have also shown that similar significant nonlinear effects persist for general three-dimensional bodies based on the extension of the theoretical analysis to a three-dimensional submerged body and by use of direct fully nonlinear numerical simulations for a realistic ship hull. The findings of the present study indicate that it is of importance to take into account the cubic self-interactions of resonant waves in order to obtain the complete leading-order seakeeping solution near the critical frequency for two- and three-dimensional submerged or floating bodies. We finally remark that the present studies were limited to the context of potential flow assumptions. Non-potential-flow factors such as viscosity and vorticity were not considered.

Acknowledgement

This research is supported financially by grants from the Office of Naval Research (N00014-16-1-3105; N00014-15-1-2460).

REFERENCES

AKYLAS, T. R. 1984 On the excitation of nonlinear water waves by a moving pressure distribution oscillating at resonant frequency. *Phys. Fluids* **27**, 2803–2807.

ALAM, M.-R, LIU, Y. & YUE, D. K. P. 2009 Waves due to an oscillating and translating disturbance in a two-layer density-stratified fluid. *J. Engng Maths* **65**, 179–200.

ALAM, M.-R, LIU, Y. & YUE, D. K. P. 2011 Resonant-wave signature of an oscillating and translating disturbance in a two-layer density stratified fluid. *J. Fluid Mech.* **675**, 477–494.

BINGHAM, H. B. 1994 Simulating ship motions in the time domain. PhD thesis, Massachusetts Institute of Technology, Cambridge, MA.

BRACEWELL, N. 1986 *The Fourier Transform and its Applications*, vol. 31999. McGraw-Hill.

BRARD, R. 1972 The representation of a given ship form by singularity distributions when the boundary condition on the free surface is linearized. *J. Ship Res.* **16**, 79–92.

DAGAN, D. & MILOH, T. 1980 Flow past oscillating bodies at resonant frequency. In *Proc. 13th Symp. of Naval Hydrodynamics* (ed. T. Inui), pp. 355–373. The Shipbuilding Research Association of Japan.

DAGAN, D. & MILOH, T. 1982 Free-surface flow past oscillating singularities at resonant frequency. *J. Fluid Mech.* **120**, 139–154.

GRUE, J. & PALM, E. 1985 Wave radiation and wave diffraction from a submerged body in a uniform current. *J. Fluid Mech.* **151**, 257–278.

HASKIND, M. D. 1954 On wave motion of a heavy fluid. *Prikl. Mat. Mekh.* **18**, 15–26.

HAVELOCK, T. H. 1958 The effect of speed of advance upon the damping of heave and pitch. *Quart. Trans. Inst. Nav. Archit.* **100**, 131–135.

https://doi.org/10.1017/jfm.2018.322 Published online by Cambridge University Press

JOHN, F. 1950 On the motion of floating bodies. Part II. *Commun. Pure Appl. Maths* **3**, 45–101.

KRING, D. C. 1998 Ship seakeeping through the $\tau = 1/4$ critical frequency. *J. Ship Res.* **42**, 113–119.

LI, Y. & ELLINGSEN, S. Å. 2016 Multiple resonances of a moving oscillating surface disturbance on a shear current. *J. Fluid Mech.* **808**, 668–689.

LIU, Y., DOMMERMUTH, D. G. & YUE, D. K. P. 1992 A high-order spectral method for nonlinear wave–body interactions. *J. Fluid Mech.* **245**, 115–136.

LIU, Y., XUE, M. & YUE, D. K. P. 2001 Computations of fully nonlinear three-dimensional wave–wave and wave–body interactions. Part 2. Nonlinear waves and forces on a body. *J. Fluid Mech.* **438**, 41–66.

LIU, Y. & YUE, D. K. P. 1993 On the solution near the critical frequency for an oscillating and translating body in or near free surface. *J. Fluid Mech.* **254**, 251–266.

MARUO, H. 1967 Application of the slender body theory to the longitudinal motion of ships among waves. *Bull. Fac. Engng Yokohama Natl Univ.* **16**, 29–61.

MO, A. & PALM, E. 1987 On radiated and scattered waves from a submerged elliptic cylinder in a uniform current. *J. Ship Res.* **31**, 23–33.

NAKOS, D. E. & SCLAVOUNOS, P. D. 1990 Ship motions by a three-dimensional Rankine panel method. In *Proc. 18th Symp. of Naval Hydrodynamics*, pp. 21–44. National Academy Press.

NEWMAN, J. N. 1978 The theory of ship motions. *Adv. Appl. Mech.* **18**, 221–283.

PALM, E. & GRUE, J. 1999 On the wave field due to a moving body performing oscillations in the vicinity of the critical frequency. *J. Engng Maths* **35**, 219–232.

SCLAVOUNOS, P. D., NAKOS, D. E. & HUANG, Y. 1993 Seakeeping and wave induced loads on ship with flare by a Rankine panel method. In *Proc. 6th Int. Conf. on Numerical Ship Hydrodynamics*, p. 62. National Academy Press.

SHEN, M. & LIU, Y. 2017 Current effects on global motions of a floating platform in waves. *Ocean Syst. Engng* **7**, 121–141.

TYVAND, P. A. & TORHEIM, T. 2012 Surface waves from bottom vibrations in uniform open-channel flow. *Eur. J. Mech. (*B*/Fluids)* **36**, 39–47.

WEHAUSEN, J. W. & LAITONE, E. V. 1960 Surface waves. In *Encyclopedia of Physics* (ed. S. Flugge), pp. 446–778. Springer.

YAN, H. & LIU, Y. 2011 An efficient high-order boundary element method for nonlinear wave–wave and wave–body interactions. *J. Comput. Phys.* **230**, 402–424.

ZHANG, Y. & ZHU, S. 1995 Resonant interaction between a uniform current and an oscillating object. *Appl. Ocean. Res.* **17**, 259–264.

ZHU, Q., LIU, Y. & YUE, D. K. P. 2006 Dynamics of a three-dimensional oscillating foil near the free surface. *AIAA J.* **12**, 2997–3009.

https://doi.org/10.1017/jfm.2018.322 Published online by Cambridge University Press